Variability of the Outer Wind Profiles of Western North Pacific Typhoons: Classifications and Techniques for Analysis and Forecasting

STEPHEN B. COCKS AND WILLIAM M. GRAY

Department of Atmospheric Science, Colorado State University, Fort Collins, Colorado

(Manuscript received 14 September 2001, in final form 31 December 2001)

ABSTRACT

The hazard posed by tropical cyclones (TCs) is often quantified in terms of the minimum central pressure (MCP) or maximum wind speed. While significant, these qualities must be balanced against considerations for the strength and spatial extent of the outer-core circulation, which also significantly determines the total peril posed by these storms. To this end, the results of recent studies on the time evolution of the outer wind structure of western North Pacific typhoons are presented. The results include a technique for diagnosing the azimuthally averaged wind profile from a combination of regional synoptic data and estimates of MCP. Aircraft reconnaissance data, augmented with available synoptic and scatterometer data, are used to determine the radial extent of 15 (R15), 25 (R25), and 33 (R33) m s^{-1} winds for 50 typhoons. Thirty-five of these typhoons were designated as the developmental dataset and 15 were reserved for use as independent data.

Using the developmental data, concurrent time series were constructed for outer wind radii and MCP values for TCs whose life cycles were unperturbed by proximity to land. Analysis of these time series revealed a distinct type of TC with very large R15 and weak intensity values. These ''gyre'' systems were examined as a special TC class. The remaining TCs were divided according to the size of their outer circulations into groups termed small, medium, and large. Observations stratified for these size categories revealed that for about 40% of the TCs, significant increases of R15 [greater than 50 km day^{-1}] occurred during the 1.5-day period before maximum intensity. Composite analyses revealed that mature large (small) TCs develop as larger (smaller) TCs early in their life cycle. Composite analysis of the gyre systems showed several unusual characteristics including very large initial R15 values (much larger than even large TCs) and weak intensities. Spatial analyses indicate that the gyre and larger TCs tend to attain maximum R15 values in locations west of 135°E whereas the smaller TCs tend to maximize farther east. Analyses of surface pressure showed that the gyres are associated with broad areas of comparatively low pressure (versus other TCs), in agreement with previous studies.

Statistical associations between R15 values and an array of environmental parameters revealed that although area coverage of intense convection was poorly correlated with R15, the radial extent of the 1004-hPa isobar (ER04) enveloping the systems was well correlated with R15. Whereas the overall relationship between MCP and R15 is weak, it is noted that when data for the gyre TCs are removed (14% of the observations), the total variance explained between MCP and R15 is more than doubled. Consequently, a regression equation using both MCP and ER04 was developed and used in conjunction with a Rankine vortex model to successfully estimate values for R15 and R25. The independent data were used to evaluate this analysis technique versus a procedure used by the Joint Typhoon Warning Center (the Huntley method) for estimating the radius of 17 m s^{-1} winds (R17). The new ER04/MCP-based technique created in this study suffered no loss of skill when applied to the independent data and both methods appear to be quite useful for estimating the properties of symmetric outer wind profiles of northwest Pacific typhoons.

1. Introduction

Some northwest Pacific tropical cyclones (TCs) develop into the largest, most powerful storms on the face of the earth, causing significant loss of property and life each year. The methods used for measuring the size and intensity of these storms have undergone basic changes in recent years. In particular, until discontinued in 1987, aircraft reconnaissance was utilized for determining the intensity and spatial extent of northwest Pacific TCs. Eliminating the aircraft observation program dictated that fixed location synoptic measurements and satellite data would become crucial for assessing typhoon size and intensity parameters. The work described in this paper utilizes the existing (pre-1987) aircraft observations to develop methods for better utilizing data from the remaining synoptic and satellite observation platforms to more reliable analyses and forecasts the spatial extent of TC strength winds.

Dvorak (1975, 1984) developed a scheme based on satellite imagery that has been successfully used by forecasters to estimate TC intensity from visible and infrared

Corresponding author address: Dr. William Gray, Dept. of Atmospheric Science, Colorado State University, Fort Collins, CO 80523.
E-mail: barb@tutt.atmos.colostate.edu

imagery using a set of empirically determined rules. However, regardless of the accuracy of these intensity estimates, difficulties remain for accurately determining the spatial properties of TC outer wind profiles. Although advanced satellite technology such as the active microwave sounder, or ''scatterometer'' (Hawkins and Black 1983), has helped greatly in estimating typhoon wind characteristics, applicable data still tend to be sparse and sporadic in nature. Agencies responsible for providing estimates of the distribution of dangerous winds (e.g., the Joint Typhoon Warning Center, or JTWC) continue to rely on a mix of ''as available'' surface ship, buoy, and island observations, as well as perspectives from composite climatologies of TC wind reports. Yet it is the radial extent of the gale force winds that is most important to affected interests. In landfall events, precise knowledge of when gale force winds will reach the coast is critical for emergency preparations.

Several prior studies have considered the size evolution of TC circulations. Using the radius of the outer closed isobar (ROCI) bounding each storm as an index of comparative size, Brand (1972) found that comparatively small Pacific TCs tended to occur during February whereas the largest TCs occurred during October. Frank and Gray (1980) used rawinsonde compositing methods to deduce that, on average, a motion-linked asymmetry exists for TCs wherein the strongest outer winds are usually located to the right of the motion vector. Merrill (1984) found that the size of Atlantic TCs as measured by the ROCI is fairly constant for westward moving storms but tends to become larger with northward motion. The latter typically occurs as these TCs approach slow-moving troughs located between the subtropical and polar anticyclones. Merrill also found little relationship between ROCI and maximum wind speeds for both Atlantic and Pacific TCs.

An in-depth analysis of TC outer wind structure by Weatherford and Gray (1988a,b) was based entirely on aircraft reconnaissance data. In these studies Weatherford and Gray derived an ''outer core strength'' (OCS) parameter for the average wind speed in the region extending from 1.0° to 2.5° latitude from the centers of tropical cyclones. This OCS parameter was found to be highly correlated with the radius of 15 m s^{-1} winds (R15) as measured by aircraft. However, changes of OCS during intensification were observed to be small as compared to changes in minimum central pressure (MCP), thereby indicating a poor relationship between time variations of OCS and MCP. As OCS and R15 were well correlated, it was inferred that relationships between R15 and intensity expressed as MCP were likely poor. The OCS also appeared to be poorly related to the TC's motion vector, implying thereby that R15 was unrelated to TC motion. Using these results, Weatherford and Gray (1988a) derived a set of average radial wind profiles for typhoons of various intensities (their Fig. 12). One property of these outer radius wind profiles was that they indicated very little change of R15 for TCs of typhoon intensity or greater. Carr and Elsberry (1997) proposed a model of tangential wind distribution to estimate outer radius wind profiles that was based on the approximate conservation of angular momentum. Using the outer wind profiles developed by Weatherford and Gray (1988a), it was assumed that the outer wind profile remains essentially static once typhoon intensity is attained.

Diagnosing and forecasting the strength and extent of TC outer wind structure are especially difficult tasks where changing synoptic environments can cause peculiar modes of variability. For example, differing environmental conditions often lead to typhoons of similar size with vastly different intensities. Specific cases include Supertyphoon Abby and Typhoon Orchid, both of which had MCP values of 930 hPa at one point in their respective life cycles. Yet Abby had a large average R15 of 520 km whereas Orchid had an average R15 of only 230 km. Conversely, Supertyphoon Vanessa at one point had an R15 value of 541 km (slightly larger than Abby 520 km) but with an MCP of 888 hPa (42 hPa lower than Abby).

In the following analyses, we group our TC data into small, medium, and large size classes, based on the peak R15 value attained during each life cycle. We also set aside for special examination a group of TCs, denoted as gyres, which had qualities distinct from the other TCs in the dataset. Changes of R15 and R25 (i.e., 15 and 25 m s^{-1} winds) with time are examined prior to and immediately after maximum intensity (MI) and the results considered in light of the current hypothesis that little variation occurs in these parameters during this stage of intensification. Composite life cycles are created to investigate differences among the size categories. The latter results show evidence for certain synoptic features being associated with the gyre and larger TCs. A useful statistical relationship is shown to occur between R15 and the radial extent of the 1004-hPa isobar (ER04) developed from analyses of surface synoptic data. We also reexamine the relationship between MCP and R15 whereby better correlations are shown to exist when data for gyre TCs are removed from the analysis. Using this information, a diagnostic equation was developed for estimating outer wind profiles wherein comparisons are made with other analysis techniques used in the western Pacific.

2. Approach

a. Data

The intensity and outer wind characteristics of western Pacific typhoons were analyzed, classified, and later composited. Tracks and center positions of TCs with similar outer wind characteristics were first examined for preferred locations of formation and movement. To accomplish this, more than 500 aircraft reconnaissance mission reports, 700 synoptic weather maps, and 20

scatterometer passes were reviewed to assess the associations between intensity (i.e., MCP), outer wind structure, size, and surface synoptic pressure patterns for 35 typhoons that occurred in the northwest Pacific during the 6 yr spanning 1980–87. An additional 15 typhoons were reserved as independent data for testing the findings of the analysis. Wind and geopotential height data at the 700-hPa level were collected by U.S. Air Force typhoon reconnaissance missions using WC-130 aircraft. Weatherford and Gray (1988a) describe details of how these missions were flown and of flight data collection techniques.

Flight data were processed with observations initially navigated to a common heading following the center of each moving TC. This procedure yielded plots of wind speed and direction for each TC in natural coordinates relative to the earth's surface (see details in Weatherford 1985, 1989). Flight data coverage typically extended radially only 400 km from the center of each TC, thereby artificially restricting the radius of 15 m s^{-1} winds for the TCs larger than 400-km radius. To alleviate this constraint additional surface and 700-hPa synoptic observations from Japanese Meteorological Agency (JMA) synoptic weather maps were consulted to supplement the aircraft reconnaissance data in analyzing the outer wind structure. Surface observations on the JMA maps were available each day at 1200 and 0000 UTC whereas 700-hPa observations were available for 1200 UTC only. Since the flight level of the reconnaissance aircraft was 700 hPa, first preference in defining conditions was given to the 700-hPa rawinsonde observations. A disadvantage associated with augmenting the aircraft data in this way lies in the possibility of overestimating the outer extent of 15 m s^{-1} (and occasionally 25 m s^{-1}) winds in areas where gaps exist between synoptic and aircraft reconnaissance data. However, the authors deemed the advantages of augmenting the data far outweighed the disadvantages and the values for R15, R25, and R33 winds were analyzed using the enhanced dataset.

To adjust the aircraft and rawindsonde data, surface wind speed values were assumed to be 85% of the values observed at 700 hPa (Frank and Gray 1980). An outer wind radius value was assigned only if the area of observed 15, 25, or 33 m s^{-1} winds (as appropriate) wrapped at least halfway around the center of the vortex. Where this requirement was met R15, R25, and R33 values were averaged azimuthally, typically over four to eight observation points, about the TC's center. In addition to wind speed and direction, the reconnaissance flights recorded the minimum 700-hPa height value obtained at storm center. Weatherford (1989) found that minimum 700-hPa height and MCP values are very well correlated such that values for minimum 700-hPa heights observed at the TC center could be converted to MCP values using the empirical formula given below where MCP is in hectopascals and HT is 700-hPa height in meters:

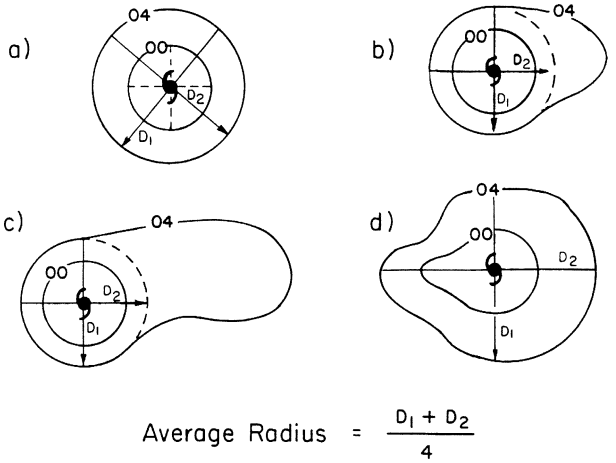

FIG. 1. Schematic showing techniques used for specifying the two outer closed isobars around tropical cyclones, in this case, the 1000- and 1004-hPa isobars (details in text).

$$\text{MCP} = 0.114 \cdot \text{HT} + 647.3. \quad (1)$$

b. TC size parameters

Merrill (1984) used ROCI values diagnosed from the ambient pressure field as a means for specifying TC size. However, neither the pressure field of the TC nor its environment are static and, therefore, any outer-closed isobar (OCI) value so designated may variously ''open'' and ''close'' in time, resulting in the immediate formation of a new ROCI with a different isobaric value. These considerations complicate the use of ROCI values for evaluating temporal changes of tropical cyclone size or correlating these size changes with changes of R15. Observations show that as R15 expands, ROCI measurements may variously indicate contraction, expansion, or no change at all. An alternative approach that is used here considers using the radii of specific fixed isobaric values encircling the TC as a size parameter. Hence, rather than trying to assess if the outer closed isobar of a TC is for example, either 1006 or 1008 hPa, the analyst simply moves directly to assess the diameter of (for example) the 1004-hPa isobar around the storm. In this way, size changes can be continuously expressed in terms of changes in the diameter of the 1004-hPa isobar over time.

Approximately 350 surface synoptic maps were inspected in estimating time variations of the outer two closed isobars about each TC center. As illustrated in Fig. 1, the average radius of these isobars was initially measured and expressed in degrees latitude for all the TCs in the dataset. If the outer two closed isobars of the TC were distinct and symmetric, then the semimajor and semiminor axes were averaged to determine a mean radius as shown in Fig. 1a. Occasionally an OCI was observed to be distinctly asymmetric in a preferred direction while nevertheless encircling more than 270° of

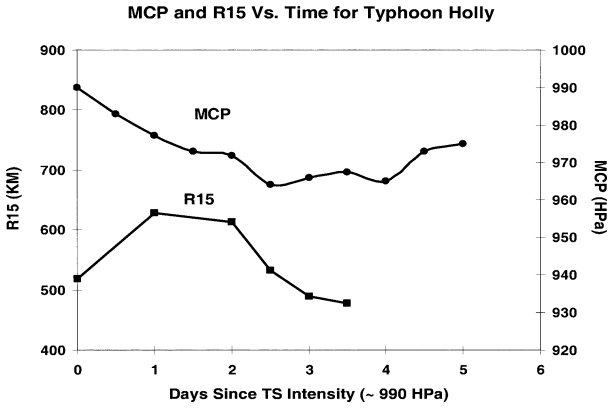

FIG. 2. Plots of MCP and R15 vs time (in days) following TC intensity (990 hPa) for Typhoon Holly, a typical gyrelike tropical cyclone.

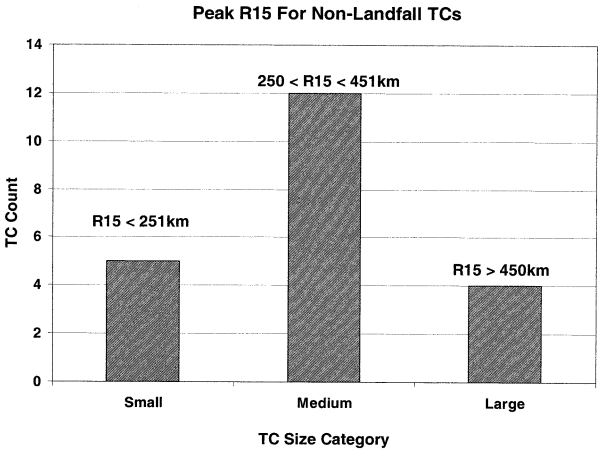

FIG. 3. Three-category size distribution of nonlandfalling TCs (gyres are excluded). Size criteria for each group are indicated.

azimuth around the cyclone. In these cases, the asymmetric isobar was truncated and retraced to approximate a symmetric inner closed isobar and an outer isobaric radius as shown in Fig. 1b. Generally, a radial measurement was recorded only if there was at least one nearby surface observation to justify the specification of an outer closed isobar. The assumption was made that a symmetric pressure gradient existed unless the data clearly indicated otherwise. Twelve-hour running means were used to smooth diurnal variations in the data. Finally, the OCI measurements were adjusted by the cosine of the latitude to account for latitudinal convergence and for slight imperfections in the stereographic representation of the JMA synoptic maps from which the data were read.

All together 725 OCI measurements were made. Of these approximately 45% were measurements wherein the isobaric value of the outer closed isobar was 1004 hPa, making this the most common closed isobaric value in the dataset. In about 85% of the cases one of the two outer closed isobars bounding the TCs had a value of 1004 hPa. Nonetheless, the 15% of the cases wherein the 1004-hPa isobar was not present points to the need for a more flexible (than OCI) size parameter for diagnosing changes in the synoptic size of a TC. This parameter needs to be consistent with size changes in R15 but not dependent on the presence of a particular isobaric value. Nine TCs that interacted with land prior to or during maximum intensity were removed from the developmental dataset. The remaining 26 TCs were designated as ''nonlandfall'' TCs and used for the composite analysis described in section 3.

Closer examination of the nonlandfall cases revealed a class of TCs that were quite different than the rest. These particular TCs had R15 values of 300 km 1 day after reaching tropical storm intensity. The latter class of TCs, termed gyres, were previously documented by Lander (1994) and are noteworthy here in that they develop from a monsoon depression or within a monsoon gyre circulation [(both formation processes are described by Lander (1994, 1996)]. In the latter, monsoon gyre case, the initial monsoon circulation eventually takes the form of a giant TC. The R15 values of the gyre TCs tended to remain large (though significant changes were possible) while MCP typically fell only to modest values. Indeed, the lowest MCP observed for this class of TCs was only 950 hPa with an average MCP of around 960 hPa. Qualitative examination of synoptic maps associated with these TCs also revealed unique characteristics including very large regions of gale force winds, at times surrounding an area of relatively light winds near the center. In the present study, TCs with R15 $\geq$ 300 km by the end of the first day after attaining tropical storm intensity (MCP of 990 hPa) were classified as gyre TCs. As only five TCs in the dataset fit this classification, this type of system appears to be somewhat rare. Four out the six largest TCs in the dataset for this study were gyres as shown in the example in Fig. 2. Note in Fig. 2 that the initial R15 value for Typhoon Holly was more than 500 km as MCP dropped below 990 hPa. Because of their unique characteristics, the gyre TCs were treated as a distinct class and separated from the other nonlandfall TCs.

A size distribution based on nonlandfall TCs (excluding gyres) was created by first calculating the mean peak R15 value (i.e., 350 km) for all TCs in the dataset. Those TCs that were within approximately one standard deviation of the mean (100 km) were classified as ''medium'' sized and TCs with peak R15 values which were either more than one standard deviation above or below the mean were classified as ''large'' or ''small,'' respectively. The latter TC size distribution, excluding gyre TCs, is summarized in Fig. 3.

3. Results

a. Properties of R15 versus intensity in relatively large and small TCs

The time evolution of the TC outer wind structure versus intensity was examined in comparative analyses

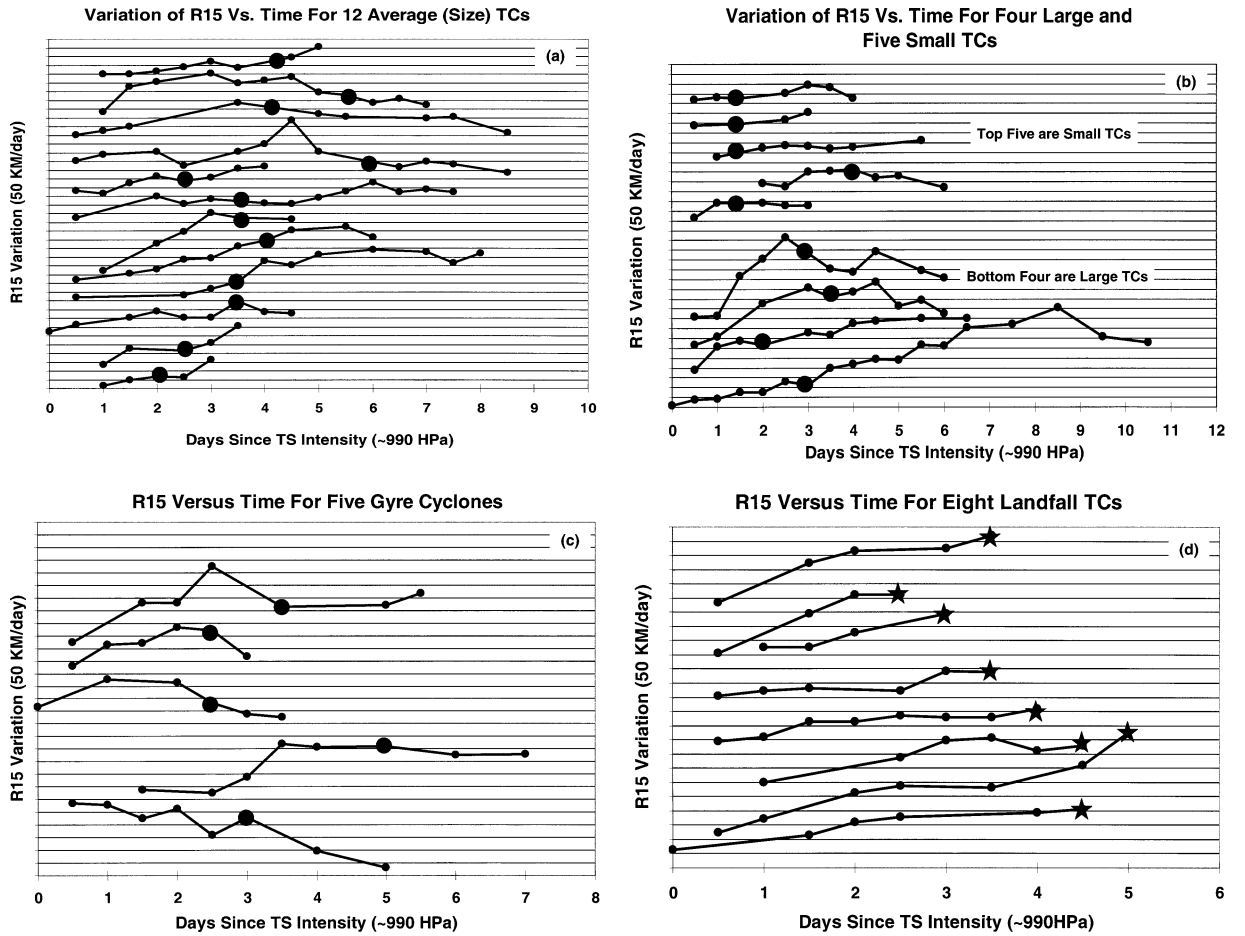

FIG. 4. Comparison of day-to-day variations of R15 and MCP for (a) medium, (b) small and large, and (c) gyre TCs, as well as (d) TCs that interacted with land. Large black circles denote the time of maximum intensity and black stars indicate landfall. Tick marks on the ordinate indicate 50 km day^{-1} change of R15, thereby offering a qualitative summary of the time varying properties of interest in the dataset.

of time series of R15, R25, and MCP for individual TCs stratified by size. Figures 4a–d and 5a,b show comparative time series plots of R15 and R25, respectively. Note that these results include gyres as well as TCs that interacted with land before reaching maximum intensity (Fig. 4d). The scale on each ordinate axis in Figs. 4 and 5 is expressed as arbitrary increments of 50 km (for R15) and 25 km (for R25), thus emphasizing change with time rather than the absolute magnitude of the radii. This way, all TCs for each category could be observed in a single plot to allow comparison of the variable total and time rates of change of R15 and R25. The approximate change with time of the different radii can be determined by noting the total number of horizontal lines crossed in time where each line denotes a distance of either 50 or 25 km in a given period of time (1 day). Large black dots indicate the point in time where each TC reached its maximum intensity. Black stars indicate when TC cores began to interact with land, thereby interrupting the life cycle. Inspection of Figs. 4 and 5 offers insight on the variability and time evolution of the TC outer core region.

A summary of the changes in R15 and R25 for 1.5 days before and after maximum intensity is shown in Table 1. Forty-three percent of the TCs exhibited R15 characteristics similar to the classical Atlantic hurricane model discussed in Merrill (1984) wherein R15 exhibits only modest or no change (less than 50 km day^{-1}) just prior to maximum intensity. Twenty-three percent of TCs showed very modest or no change (less than 30 km day^{-1}) of R25 within 1.5 days prior to maximum intensity (note that the number of TCs sampled for R25 is small due to sparse data during this time frame).

There are, however, some notable departures from Merrill's conceptual model in Figs. 4 and 5. In particular, 38% (10/26) of the TCs exhibited R15 changes greater than 50 km day^{-1} and 19% (5/26) exhibited greater than a 100 km day^{-1}. Though 15% (4/26) of TCs exhibited R25 changes greater than 30 km day^{-1}, it is difficult to assess if these values would have been greater in a larger data sample. In each of these cases, R15 and R25 changes were occurring during intensification. The authors speculate that the sudden changes in R15 and R25 that appear in Figs. 4 and 5 may be related to interactions

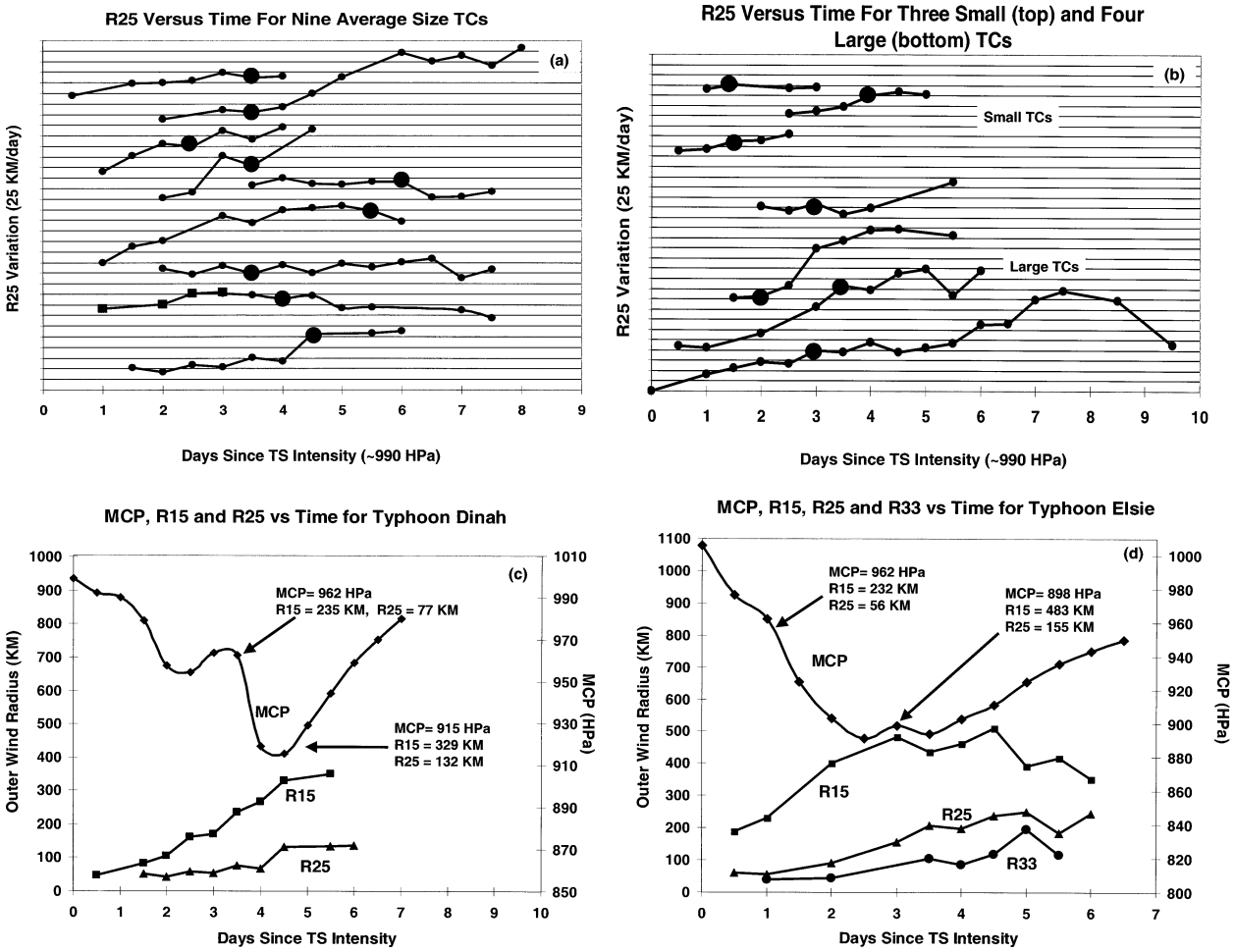

FIG. 5. As in Fig. 4 but for comparison of day-to-day variations of R25 for small, medium, large, and gyre TCs but where divisions on the ordinate scale indicate 25 km day^{-1} changes. (c) and (d) Large changes in R15, R25, and MCP during periods of intensification for Typhoon Dinah and Supertyphoon Elsie. Note in (c) and (d) that the left ordinate shows R15/R25 in km and the right ordinate scales the time series of MCP in hPa.

between the TC's outer core and the synoptic environment.

No distinct relationship was noted between R15 and R25 changes and TC size. Nevertheless, the evidence shown in Figs. 4 and 5 constitutes a significant departure from the conventional conceptual model wherein outer wind structure changes little during intensification (e.g., Weatherford and Gray 1988b; Carr and Elsberry 1997).

Changes of R15 and R25 also occurred while MCP was falling rapidly as shown in Figs. 5c,d. Returning to Table 1, we find that within 1.5 days following maximum intensity, 58% of the TCs showed little R15 change (less than 50 km day^{-1}). The data do not reflect later size changes when TCs undergo extratropical transition. For the TCs sampled, none underwent extratropical transition within 1.5 days after MI. What the data do show is that, on average, the TCs outer wind structure does not change much immediately following maximum intensity. Some TCs reached peak R15 at MI or several days prior, then contracted, while other TCs exhibited R15 expansion well past MI. Similar tendencies are discernible in the R25 graphs and (though less so) in R33 graphs (not shown).

Figures 4 and 5 illustrate that for an appreciable fraction of these TCs, there are significant changes in the outer core during intensification. The inference that R15 expansion generally occurs primarily during the tropical storm and minimal typhoon intensities was based on interpretations of results in Weatherford and Gray (1988b), which showed, on average, very little change in the R15 once typhoon intensity was obtained. However, it appears that broad statistical averaging methods used in that study likely masked the time varying qualities of individual TCs. Using Weatherford's (1989) OCS versus MCP data, the change in the OCS was determined during the intensification stage of 39 typhoons. Next, the change in the R15 was calculated using Weatherford and Gray's (1988b) relationship [their Eq. (1a)] as follows:

$$R15 = 20\ \mathrm{OCS} - 150.8. \qquad (2)$$

TABLE 1. Number of TCs and percentage of the nonlandfall cases exhibiting R15/R25 changes averaging less than 50 (30), greater than 50 (30), and greater than 100 (50) km day^{-1} within 1.5 days before and after maximum intensity (MI). Some change values could not be calculated for lack of sufficient data.

	ΔR15 < 50	$50 < \Delta$R15 < 100	ΔR15 > 100	Gyres
Before MI	11	5	5	5
Percent of dataset	43	19	19	19
After MI	15	0	4	7
Percent of dataset	58	0	15	27
	ΔR25 < 30	$30 < \Delta$R25 < 50	ΔR25 > 50	Gyres
Before MI	6	2	3	15
Percent of dataset	23	8	12	57
After MI	8	1	3	14
Percent of dataset	31	4	12	53

Here, R15 is expressed in kilometers and OCS (i.e., the mean tangential wind between 1°–2.5° radius) is given in meters per second. The time derivative of Eq. (2) can be represented as

$$D(R15) = 20D(\text{OCS}), \quad (3)$$

where D(R15) is the change in R15 in kilometers per day and D(OCS) is the time change in OCS expressed in meters per second per day. Using Eq. (3), the change in R15 was calculated over the time period during which intensification took place to obtain the change in R15 as kilometers per day. The results of this exercise are shown in Table 2.

Just over half (54%) of the TCs in Table 2 exhibited R15 changes greater than 35 km day^{-1} during intensification while a third exhibited changes greater than 50 km day^{-1}. It is clear that, even in Weatherford's (1989) data, at least a third of the TCs exhibited R15 changes greater than 50 km day^{-1} during intensification.

Clearly, forecasters must not assume that the radial extent of the TC's gale force wind distribution will remain fixed throughout intensification. Consider for example, Dvorak's (1975, 1984) results showing that, on average, TCs may go from tropical storm intensity to typhoon intensity in roughly 1.5 days. If this same TC had an initial R15 of 100 km (at tropical storm intensity) and expanded 50 km per day, it would then have an R15 of 175 km by the time it attained typhoon intensity, thereby nearly doubling its size.

b. *Composite analyses of gyre and large and small TC life cycles*

Comparative time series composites of the time evolution of the outer wind structure and MCP were created for gyre TCs and for each of the three size categories noted previously. These composites were used in further examining how R15, R25, and R33 change with time and in relation to MCP. The composite life cycles spanned the time of MCP for each TC type. In each case, the life cycle began when the MCP of each TC reached 990 hPa, extended through maximum intensity, and ended as rising MCP neared 980 hPa. These bounds effectively maximized the data available from the aircraft reconnaissance observations.

TABLE 2. Incidence of typhoons in each size classification exhibiting prescribed values of OCS and R15 change during TC intensification using Eq. (3).

No. of storms	Percent of total sample (39 storms)	Change in OCS [(m s^{-1}) day^{-1}]	Change in R15 (km day^{-1})
18	46	<4	<35
21	54	≥ 4	≥ 35
13	33	≥ 6	≥ 50
4	10	≥ 8	≥ 75

A problem arose in merging the life cycles of individual TCs, each of which persisted for specific and notably different lengths of time; Supertyphoon Abby's life cycle spanned 11 days while Typhoon Orchid lasted only 6. To accommodate these differences, a normalized life cycle timescale variable was defined as given by

$$\text{Percent of Life Cycle} = (\text{DTS})/(\text{TT}) \cdot 100. \quad (4)$$

Here, DTS represents the approximate number of days of elapsed time since a given TC initially gained tropical storm intensity (990 hPa) and TT is the final total time duration (in days) of the TC's life cycle. Note that the time of maximum intensity in relation to these bounds is not a consideration for the life cycle scaling.

Utilizing the normalized time variable as specified by Eq. (4), composite life cycle time series were created for the three TC size categories and gyres as shown in Figs. 6a–d. On average, the medium TCs (Fig. 6a) reached TC intensity with an R15 value of approximately 130 km, which then increased to more than twice that value by maximum intensity. The R15 values in Fig. 6a show little change near MI (the lowest composite MI value being 938 hPa), and often began to decrease as MCP began to rise. Both R25 and R33 doubled in size between the 25% of life cycle point and the time of maximum intensity. After maximum intensity, R25 and R33 tend to stabilize and then disappear at the 75% point in the life cycle. Note that the tendency for a contraction in R15 and R25 just prior to maximum intensity (observed in Figs. 4a–d and 5a,b) does not occur in the composite, which has the affect of averaging out this characteristic.

Small TCs (Fig. 6b) tend to have higher MCP values in the composite life cycles wherein the lowest composite MCP value for the small TCs (961 hPa) is roughly 23 hPa higher than that for the medium TCs. Moreover, MCP change during the life cycle of the small TCs did not exhibit so steep a drop as was observed for the medium TCs. This difference may be a reflection of bias due to the limited sample size (five cases), as the authors have personally observed numerous small, but intense

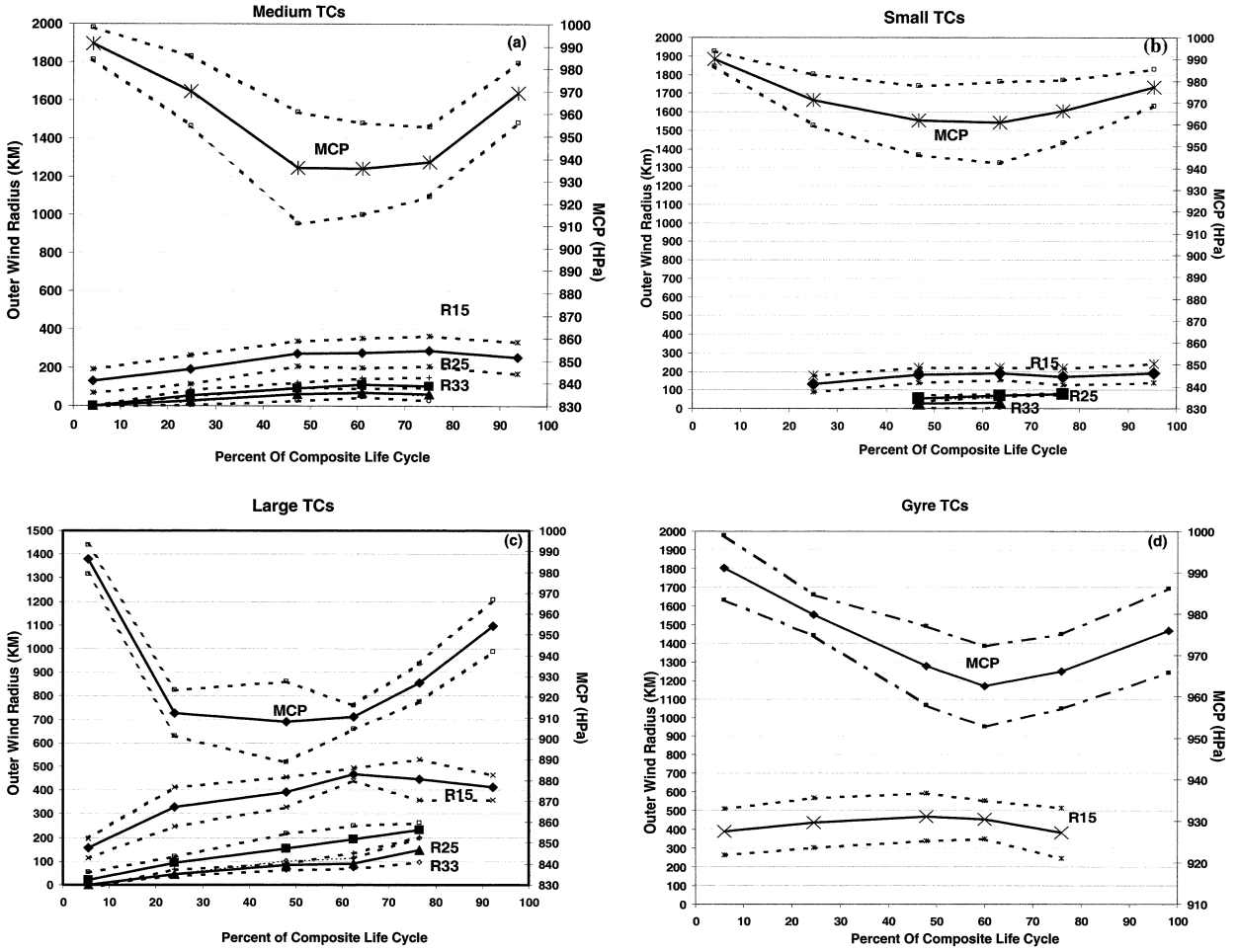

FIG. 6. Comparative composite time evolution of R15, R25, R33, and MCP for (a) medium, (b) small, and (c) large size TCs, and (d) gyres. In each panel, life cycles are normalized and scaled from 0% to 100%, beginning when the storm first attains TC intensity (0%) and ending when MCP rises to 990 hPa (100%).

storms over the years. Although data were insufficient for determining R15 early in the composite small storm life cycle, the value for the 25% point is 60 km smaller than the value for the medium-sized TCs at the same point. Hence, small TCs tend to develop as small systems as compared to the medium TCs. If linear extrapolation of R15 is made in Fig. 6b between the beginning of the life cycle and the 25% point, an initial value of R15 of about 100 km can be inferred. Consequently, small TCs may also double their R15 by the time maximum intensity is attained. Overall, R15, R25, and R33 for small TCs remained essentially invariant near and after maximum intensity, similar to the medium-size TC composite.

Although the sample size for the large TCs was also limited (only four storms; see Fig. 4b), each of the TCs in the large category reached supertyphoon intensity with sustained winds greater than 67 m s^{-1}. The lowest composite MCP value for the large TCs in Fig. 6c (908 hPa) was 30 hPa lower than that of the medium TC composite and about 50 hPa lower than that for the small TCs. Additionally, the change of MCP during the composite large TC life cycle exhibited much sharper variations than did the medium TCs. Note, however, that intense typhoons do not always develop large R15 values. Four supertyphoons in the developmental dataset were classified as medium size, based on peak R15, and the authors have personally observed small-size supertyphoons as well. Overall, though the trend in this dataset was for the very intense TCs to be medium or large with the potential to become very large later in their life cycle.

Some interesting features in Fig. 6c marked the changes of R15, R25, and R33 for the four large TCs. At the beginning of the composite life cycle, R15 was only slightly larger than the values for the medium-sized TCs. However, by the 25% point in the life cycle, the large TC R15 had grown to 1.7 times larger than medium TCs and almost 2.5 times larger than the mean for the TC class. Again, it appears that the size of a TC tends to be defined near the beginning of the life cycle and, hence, may be determined by the synoptic envi-

ronment. Hence, early in the life cycle, large TCs tend to become larger than medium TCs and small TCs remain smaller than either the medium or large TCs. But, between the beginning of the life cycle and maximum intensity, R15 for large TCs increases by a factor of 2.5, significantly more than observed for small, and medium-size TCs. The mean R25 of large TCs increased by a factor of ~3 between the beginning of the life cycle and maximum intensity. It is interesting however that R33 for large and medium TCs is about the same, suggesting that in areas closer to the center of the large and medium storms, the size differences tend to decrease. Small TCs, on the other hand, exhibited R25 and R33 values only half as large as the values of the large- and medium-size TCs.

The composite of large TCs (Fig. 6c) exhibits a sharp increase of R15 as MCP falls rapidly during the 5%–25% segment of the composite life cycle. To determine if this tendency was a real feature of the composite, the R15 change for each individual large TC was examined for this feature. This analysis showed that the R15 of one of the four TCs tripled in size and biased the composite value toward a larger value although the other three TCs also exhibited sharply larger R15 values (ranging from 1.7 to 2.1 times larger) by the 25% point of the large TC composite life cycle. Apparently, the large TCs show significant increases in R15 during periods of rapid intensification, a finding (however tentative) that surprised the authors. Some expansion in R15 was expected, especially as the TC reaches minimal typhoon intensity [as found by Weatherford and Gray (1988a,b)], but not as much as was observed. Again, this tendency may be related to the TC interacting with a synoptic-scale phenomenon (such as a surge in the westerly monsoon flow) that contributed to the sharp increase in size during intensification. Finally, R15 continued to increase in value for the large TCs (albeit at slower rates) until MCP was clearly rising. Both R25 and R33 showed similar trends except that values continued to increase later (e.g., to 80%) in the life cycle. As noted previously for the small and medium TCs, the large TC composite did not pick up (i.e., smoothed out) the tendency for a slight contraction of R15 prior to maximum intensity, which was observed in three of the four large TCs (e.g., Fig. 4b).

The composite life cycle for gyre TCs shown in Fig. 6d exhibits a comparatively shallow change of MCP (similar to small TCs) but very large R15 values, similar to those for the large TCs. To facilitate direct comparisons of the gyres and the other three TC categories, the composite life cycle values of R15 and MCP for each are shown in Figs. 7a and 7b, respectively. The gyres have R15 values that are 2.5 times greater than the large TCs and 3.0 times greater than medium TCs at the beginning of the composite life cycle. In addition, the gyres remained large throughout their life cycles with respectively smaller R15 changes as compared to the large and medium TCs. Finally, the change in MCP

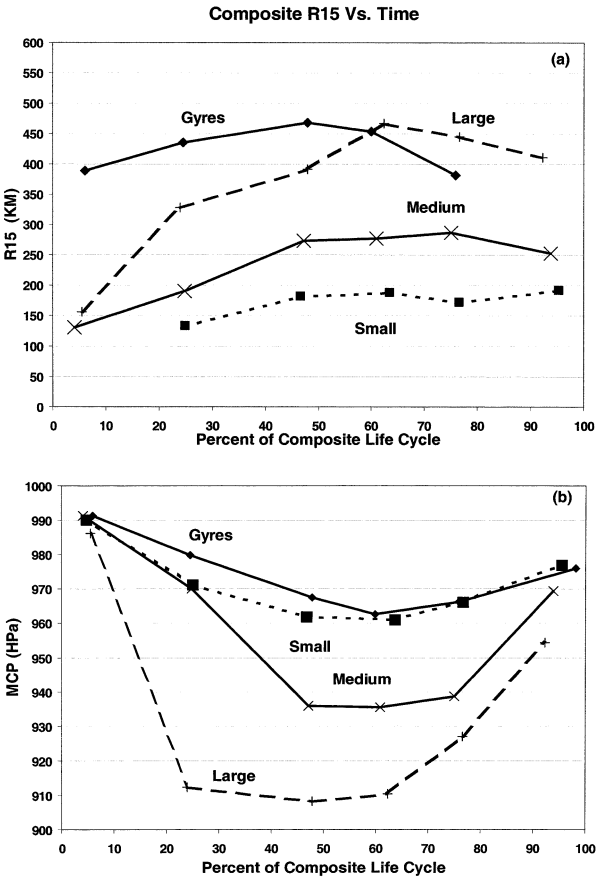

FIG. 7. Comparison of mean time variation of (a) R15 and (b) MCP over composite life cycle (0%–100%) for small, medium, and large TCs, and gyres.

for gyres (Fig. 7b) during the life cycle was weak, similar in magnitude to the values observed for the small TCs.

c. Seasonal and synoptic characteristics of large, medium, small, and gyre TCs

The main features of the time and space distributions of the TC groupings considered in this study are summarized in Figs. 8a–d. Of the nonlandfalling TCs (including gyres), 13 attained their peak R15 values after 1 October, 12 during the months of July–September, and 1 during May; the temporal distribution of occurrence thus having a slight bias toward late season TCs. Figures 8a–d show the geographical distributions of the TCs as center positions at maximum R15 labeled with the month of occurrence. Most of the medium TCs in the sample (Fig. 8a) occurred after September at positions scattered throughout the basin. Two small early season (prior to October) TCs reached maximum R15 at latitudes north of 25° whereas two others clustered at lower latitudes later in the year (Fig. 8b). All four large TCs (Fig. 8c) were located west of 135° longitude and north

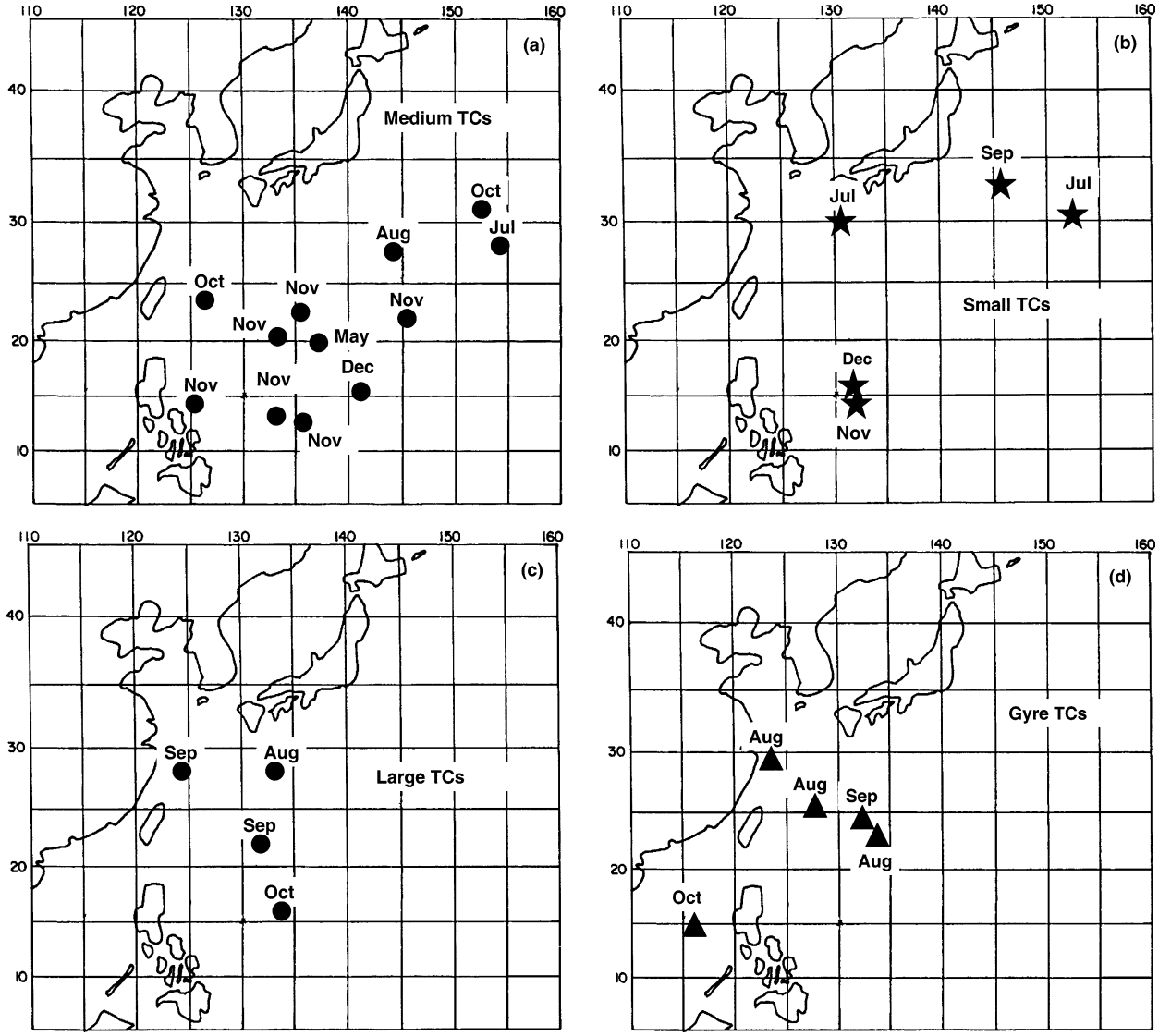

FIG. 8. Map of northwest Pacific region showing the spatial distribution of center position (and month) at peak R15 for (a) medium, (b) small, and (c) large TCs, and (d) gyres.

of 15° latitude at maximum R15. Three of the four large TCs occurred during the August and September climatological height of the season (Fig. 8c). The gyre TCs showed a spatial distribution similar to the large TCs wherein four out of five were located west of 135° longitude and north of 20° latitude (Fig. 8d).

The midseason (August and September) concentration of gyre and large TCs and their tendency to develop peak R15 values near the Asian continent (as opposed to farther east in the open ocean) suggests that favorable configurations of the monsoon circulation figure in the development of the gyres and large TCs. Case studies by Lander (1994) showed such a tendency wherein these gyre systems develop from the monsoon trough as a discrete mode of TC genesis and slowly intensify while moving westward toward the coast of southeast Asia. We expanded on these considerations by inspecting the surface pressure distribution associated with the gyre storms in the JMA weather maps. Surface pressures were read via visual inspection at distances of 445 (i.e., equivalent to 4° latitude), 890 (8°), 1330 (12°), 1775 (16°), 2220 (20°), 2665 (24°), and 3110 km (28°) from the TC centers. The configuration of the pressure field anomalies associated with the gyres are shown in Figs. 9 and 10. Surface pressure values were read along each of the radial headings heading including the 245° (west-southwest), 290° (west-northwest), 315° (northwest), 360° (north), 45° (northeast), 70° (east-northeast), and 115° (east-southeast) radials. These pressure analyses were made beginning 2 days before maximum intensity and extending through 2 days following MI. Using this information, average surface pressure patterns and

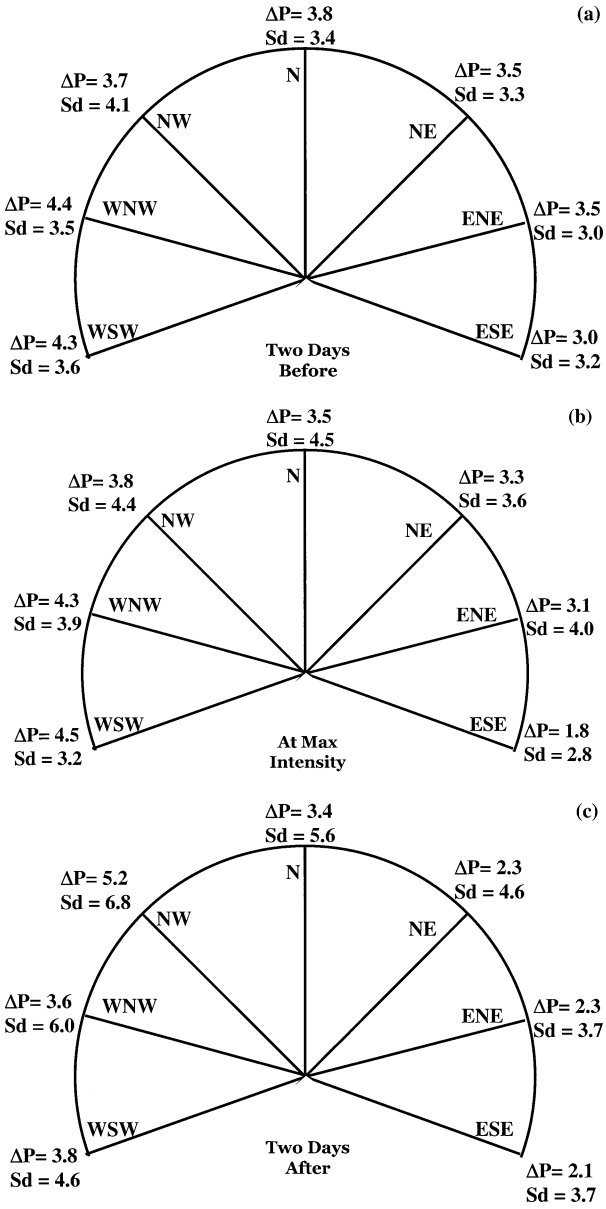

FIG. 9. (a) Schematic of mean pressure anomalies (hPa) averaged along radial arms extending 1330 km (radius) from the center of the gyre TCs for 2 days prior to maximum intensity, (b) at maximum intensity and (c) 2 days later. Here, ΔP signifies the difference between the mean gyre pressure field versus that for the mean field for all nonlandfall TCs; Sd indicates the standard deviation of pressure at six points (see text) along each radial in the mean surface pressure field for all nonlandfall TCs.

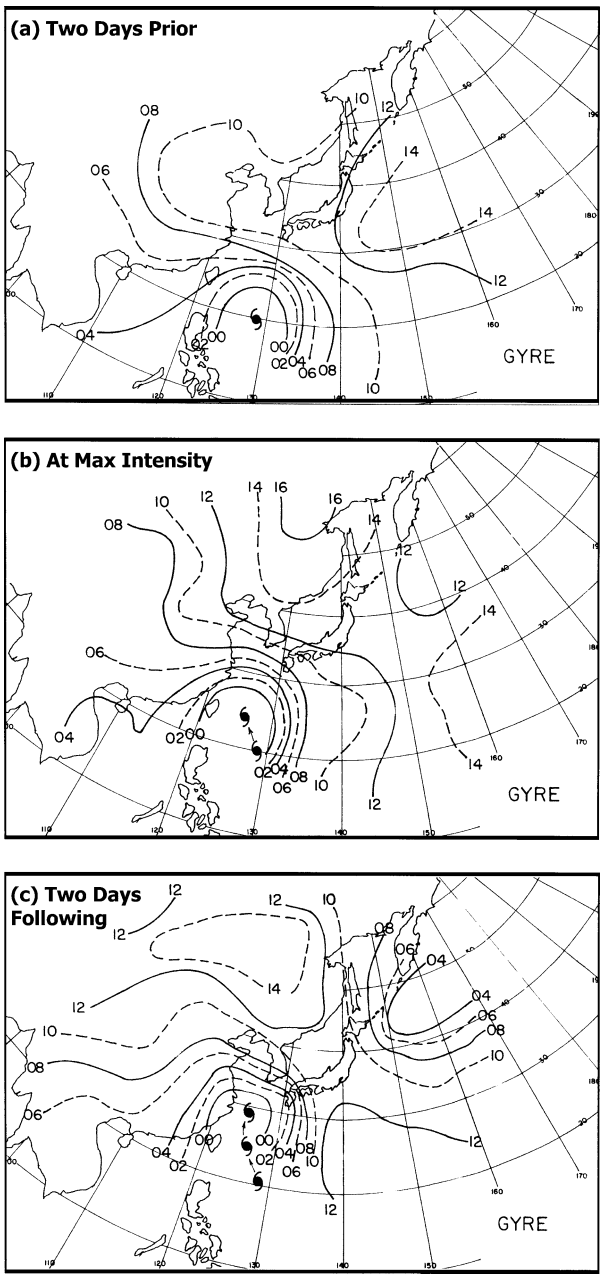

FIG. 10. Composites of the mean ambient surface pressure (+1000 hPa) surrounding the gyre TCs 2 days prior to (a) maximum intensity, (b) at maximum intensity, and (c) 2 days following maximum intensity.

anomalies were developed for the gyres and each of the other three TC size categories and included all 26 nonlandfall TCs.

Pressure anomaly fields associated with the gyre TCs before, during, and following MI were calculated by subtracting gyre average pressure at the specified directions and distances (see Fig. 9) from each TC center from the ensemble average surface pressure field obtained for the nonlandfall TCs. In a similar way the average pressure at each specified direction and distance for the small and the large TCs were subtracted from the ensemble average pressure field [not shown here; see Cocks (1997)]. The pressure anomaly values were then averaged along each radial direction at distances of 1330 (12° latitude), 2220 (20°), and 3110 km (28°) from the TC center. The resulting mean (ΔP) values for the gyre TCs are shown for the 1330-km radius in Figs.

TABLE 3. Mean pressure anomalies averaged along a 1330-km radius extending from the center of large TCs for five different observation times spanning 2 days prior until 2 days following MI. The ΔP symbol designates average pressure (difference) for medium-size TCs minus average surface pressure for large TCs (in HPa); Sd designates one standard deviation of the pressure (in hPa), averaged for six points along each radius extending from 890 to 3100 km from the center of the medium TCs (see text).

Days till MI	Medium minus large: Directions emanating from center						
	WSW	WNW	NW	N	NE	ENE	ESE
−2	$\Delta P = -0.2$	$\Delta P = -0.5$	$\Delta P = -0.4$	$\Delta P = -0.3$	$\Delta P = -0.9$	$\Delta P = -0.2$	$\Delta P = -0.2$
	Sd = 1.9	Sd = 2.6	Sd = 3.9	Sd = 2.9	Sd = 2.4	Sd = 2.5	Sd = 2.36
−1	$\Delta P = 0.7$	$\Delta P = 1.6$	$\Delta P = 2.1$	$\Delta P = 1.5$	$\Delta P = 0.3$	$\Delta P = 1.2$	$\Delta P = 1.0$
	Sd = 1.9	Sd = 2.5	Sd = 4.5	Sd = 4.3	Sd = 2.5	Sd = 2.5	Sd = 2.0
0	$\Delta P = 1.7$	$\Delta P = 3.6$	$\Delta P = 4.1$	$\Delta P = 2.8$	$\Delta P = 1.6$	$\Delta P = 2.2$	$\Delta P = 1.5$
	Sd = 2.3	Sd = 3.7	Sd = 4.5	Sd = 4.1	Sd = 3.1	Sd = 2.9	Sd = 2.4
1	$\Delta P = 4.4$	$\Delta P = 5.4$	$\Delta P = 5.6$	$\Delta P = 5.8$	$\Delta P = 4.5$	$\Delta P = 3.8$	$\Delta P = 1.3$
	Sd = 3.0	Sd = 4.5	Sd = 5.3	Sd = 4.9	Sd = 3.3	Sd = 3.6	Sd = 2.7
2	$\Delta P = 6.2$	$\Delta P = 4.9$	$\Delta P = 4.9$	$\Delta P = 5.5$	$\Delta P = 5.9$	$\Delta P = 4.5$	$\Delta P = 4.3$
	Sd = 3.9	Sd = 6.1	Sd = 6.6	Sd = 5.3	Sd = 3.5	Sd = 3.2	Sd = 3.2

9a–c. The anomaly at 1300-km radius on a given radial was considered significant if the anomaly value exceeded one standard deviation (Sd) of the ensemble averaged value for all points (i.e., for 890, 1330, 1775, 2220, 2665, and 3100 km) along that radial. Inspection of the full set of analyses (similar to) for Figs. 9a–c (not shown) for each radial distance (i.e., from 445 to 3110 km; not shown) reveals that the largest pressure field differences (i.e., largest ΔP values) associated with the gyre TCs occurred within the 1330-km radius. The gyre pressure field anomalies at 1330 km were significantly different from the mean field 2 days prior to maximum intensity (Fig. 9a) in five of the seven radial directions. At maximum intensity (Fig. 9b), significant anomalies are concentrated in the west side of the analysis although the anomalies in most other radial directions also differed by approximately one standard deviation from the average pressure field of the nonlandfall TCs. Following maximum intensity (Fig. 9c) and for radii beyond 1330 km, the pressure anomalies generally were insignificant by this criterion. This result is consistent with the differences observed between gyres and other TCs in the R15 composites (cf. Figs. 7 and 8) wherein the greatest differences occurred early in the life cycle. It was somewhat surprising however that significant pressure anomalies associated with the gyres did not extend past maximum intensity since the R15 composites (Fig. 6d) indicate that the gyres remain 175 or more kilometers larger than medium and small TCs late in the life cycle.

In a similar analysis, significant pressure field differences could not be detected when small TCs were compared to medium TCs. It is possible (perhaps likely) that the compositing technique could not resolve differences owing to the small number of cases in each sample. Some significant differences were noted between the large and medium TCs as shown in Table 3. Observe that the large positive pressure anomalies (ΔP) in Table 3 indicate that the comparatively lower pressure values surrounding the large TCs develop primarily after maximum intensity. However, large R15 differences were observed between large and medium TCs prior to maximum intensity. Hence, the lack of large pressure differences prior to MI (i.e., days -2, -1) in Table 3 was unexpected since large TCs tended to be significantly larger than the medium TCs early in the composite life cycles.

The pressure data extracted from the JMA analyses were also used to create composite surface pressure maps (Fig. 10) of the environment around gyre TCs for 2 days before, at, and 2 days following maximum intensity. These composite analyses reveal an unusually large monsoon circulation with very low surface pressures that were 5–10 hPa below the climatological values found by Sadler et al. (1987). Although it is difficult to meaningfully characterize the synoptic pattern beyond 1330 km owing to measurement uncertainty, the overall pressure pattern associated with the gyres appears to indicate an expansive monsoon and a weaker than normal subtropical high. The patterns in Fig. 10 tend to be quite different from the patterns associated with small, large, and medium TCs (not shown). In particular these features include the broad area of regional low pressure expanding into southeast Asia, the weaker subtropical ridge, and the broad low pressure area that develops northeast of the gyres 2 days after MI (see also Lander 1996).

TABLE 4. Results testing linearity of outer pressure gradient. Column headings include specific correlation test, number of observations, correlations coefficient (R), variance explained, standard errors [SD, where SE = 2(/SQRT(n)] expressed here in degrees of latitude, and the linear equation used to convert R08 and R00 to ER04 in units of degrees latitude.

Test	No. of obs.	R	Variance	SE	Conversion equation
R08 vs R04	146	0.88	0.78	0.7	ER04 = 0.75*R08 − 0.75
R00 vs R04	167	0.90	0.82	0.6	ER04 = 1.13*R00 + 1.21

4. Statistical associations involving R15

a. Statistical linkages between R15 and ER04

As noted previously in section 2b, a 1004-hPa contour was diagnosed for each TC observation. In some cases

where actual data did not show the 1004-hPa isobar, it was necessary to extrapolate from other isobaric values to obtain a virtual (i.e., equivalent) 1004-hPa radius parameter. This equivalent 1004-hPa radius parameter (ER04) was obtained via outward or inward (as appropriate) extrapolation from available measurements to an estimated isobaric radius value for 1004 hPa. Physically, this procedure assumes that the radial pressure gradients are approximately linear in the outer regions of TCs. Correlation tests utilizing radii measured with ample data coverage at 1008 hPa (R08) and at 1000 hPa (R00) versus 1004 hPa (R04) isobars confirmed the approximate validity of this assumed linearity of the outer pressure field, as shown in Table 4. The least square best fit equations in Table 4 were developed for relating both R08 and R00 to R04.

An illustration of the advantages of ER04 versus ROCI for estimating R15 is shown in Figs. 11a,b. Figure 11a shows Supertyphoon Abby with a central pressure of 930 hPa, R15 of 520 km, and ROCI of 5.7°. In comparison, Typhoon Orchid, with the same 930-hPa central pressure as Abby has a much smaller R15 (230 km) but a ROCI of about 5°, essentially equal to Abby (5.7°). Hence, whereas the R15 of Supertyphoon Abby is more than twice that of Typhoon Orchid, their ROCI values are about the same. The latter occurred because the isobaric fields surrounding the two TCs were quite different. In particular, the OCI observed for Abby was 1000 hPa while the OCI for Orchid was 1008 hPa. As a consequence of the latter, large differences occurred in ER04. As shown in Fig. 11b, ER04 for Abby is more than twice that for Orchid, consistent with the R15 ratio for two TCs.

Using the empirical equations given in Table 4, R08 and/or R00 (as appropriate) were converted to ER04 values, allowing the authors to continuously document

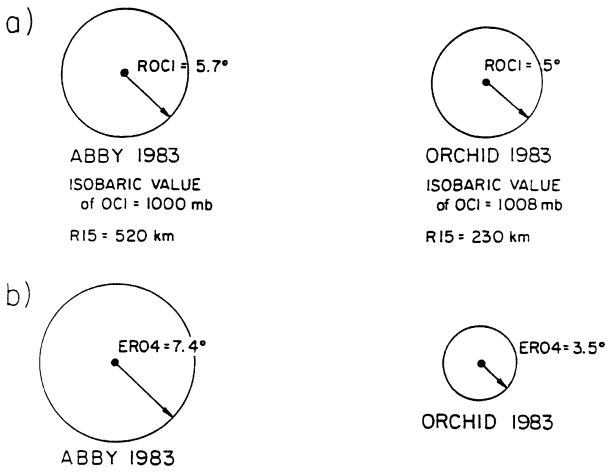

FIG. 11. Comparative schematics illustrating the critical size differences that occur for ER04 vs ROCI representative of TC size. Values plotted include ROCI, OCI isobaric value, ER04, and R15 for Supertyphoon Abby and Typhoon Orchid. (b) ER04 more clearly captures the difference in R15 between these two TCs.

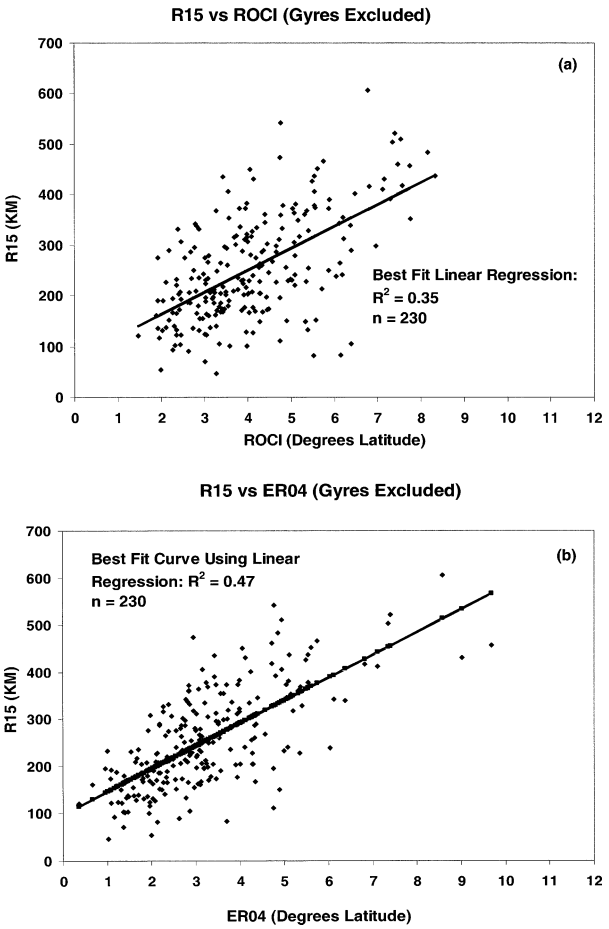

FIG. 12. Scatterplots for (a) R15 vs ROCI and (b) R15 vs ER04 for nonlandfall TCs (gyres and landfall TCs are excluded). Best fit linear regression line and parameters are shown.

all TC size changes (gyres and landfall TCs excluded) expressed in terms of a single parameter (i.e., ER04) with few data gaps throughout the entire TC life cycle. Figure 12 shows a scatterplot of the relationship between simple ROCI values and R15 wherein R15 variance explained is 35%. Excluding observations from gyres and TCs that had made landfall, a significantly stronger relationship between ER04 and R15 is obtained and shown in Fig. 12b wherein the variance explained is 47%. Nonetheless, even for the best of these results (i.e., Fig. 12b), the fraction of R15 variance explained by ER04 alone would be inadequate as a means for useful empirically estimates of R15.

Correlation tests between R25 and ER04 revealed net variance explained of 24%, a much weaker relationship than was observed for R15. Consequently, whereas ER04 is well correlated with outer wind strength as selected by R15 values, the reliability of this relationship decreases moving toward the stronger wind domains nearer the center. The latter result is physically consistent in that radial pressure gradients within de-

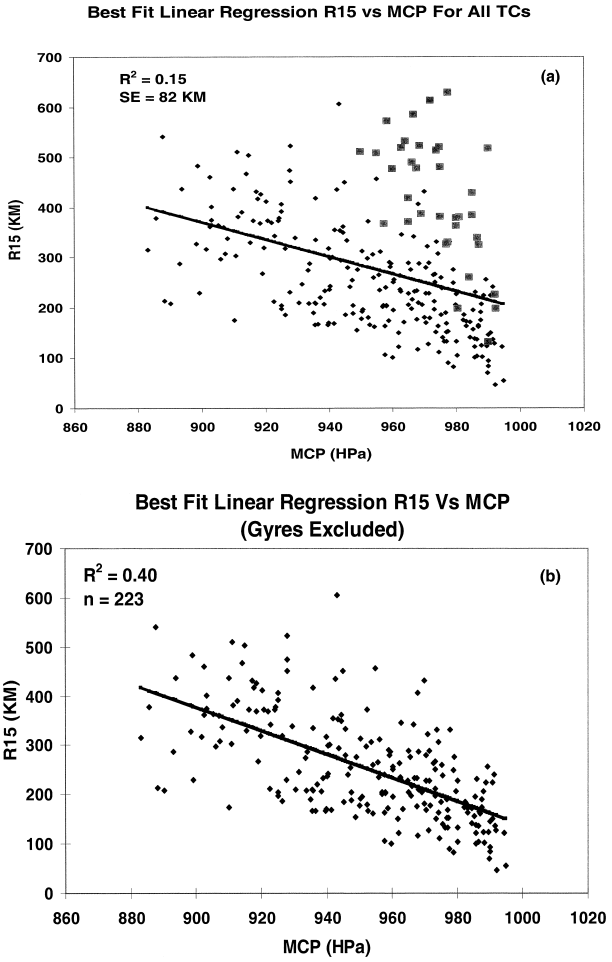

FIG. 13. (a) Scatterplot and regression analysis for R15 vs MCP for all TCs and (b) for all TCs excluding gyres. Note the substantial improvement in variance explained (r^2 increase from 0.15 to 0.40) between (a) and (b).

veloped TCs likely become increasingly nonlinear nearer the eyewall.

b. Relationships between R15 and MCP

Relationships between minimum central pressure (MCP) and R15 were reexamined to determine if the exclusion of gyre TCs would have an effect. Previously, Weatherford and Gray (1988b) reported a weak relationship ($R^2 = 0.23$) between MCP and R15. Figure 13a presents a scatterplot showing the distribution of R15 versus MCP values including gyre observations (the large squares). The net variance explained in Fig. 13a by linear least squares regression is about 15%, a significantly weaker relationship than reported by Weatherford and Gray (1988a). As was discussed in previous sections, gyres are large throughout their life cycles and are of generally lower intensity as compared to medium and large TCs. The gyres also appear to be associated with a surface pressure regime that is distinct from the other TC classes considered here. These considerations suggest that a better general relationship might exist between R15 and MCP if gyre observations are removed from the data. As shown in Fig. 13b, removing the gyre-linked observations (14% of the total data) increased the net variance explained to 40%, more than double the variance value noted in Fig. 13a for all data. We surmise that the original dataset of Weatherford and Gray (1988b) likely included some gyre TCs, causing lower variance explained for R15 versus MCP. Results from our analyses of the seasonal/synoptic conditions peculiar to each TC size class in section 3c indicated that significantly different synoptic pressure patterns were associated with gyre TCs. This information, along with the results in Figs. 13a,b, suggest that a better relationship might be observed between MCP and R15 if synoptic pressure patterns are taken into account. Although the R15 versus MCP relationship for the gyreless data in Fig. 13b is stronger than previously reported, the relationship (40% variance explained) is also inadequate for accurately estimating R15. However, as outlined in the next section, by using both MCP and ER04 as variables, a multiple regression equation can be developed to provide useful estimates of R15.

5. Techniques for estimating outer wind profiles

As both ER04 and MCP exhibit comparatively strong relationships with R15, they were chosen as candidate parameters for developing regression equations to estimate current values for R15. The TCs near landfall and gyres were removed from developmental datasets. Regression equations for estimating R15 were then developed using data for 30 different TCs throughout the various stages of their development. A test for correlation between ER04 and MCP yielded a value for variance explained of only 15%, suggesting that no strong relationships exist between these two variables. Consequently, it is likely that they can be used together in a statistical regression relationship with little chance of significant overfitting effects. Using the International Mathematics Statistics Library software package (IMSL 1987), multiple regression equations were then developed for estimating values of R15 using both ER04 and MCP as input variables. The resulting equations for estimating R15 have the following form:

$$\mathrm{R15} = 42.1 \cdot \mathrm{ER04} - 1.875 \cdot \mathrm{MCP} + 1940.5, \quad (5)$$

where ER04 is measured in degrees latitude and MCP is expressed in hectopascals. Figure 14 shows the distribution of estimated versus observed values of R15 wherein variance explained is 63% with a standard error of 64 km. This technique, in its current form, shows bias in overestimating R15 for small TCs and underestimating R15 for the larger ones.

Once an estimate for R15 was obtained, values for R25 and R33 were also estimated using established relationships developed previously by Hughes (1952),

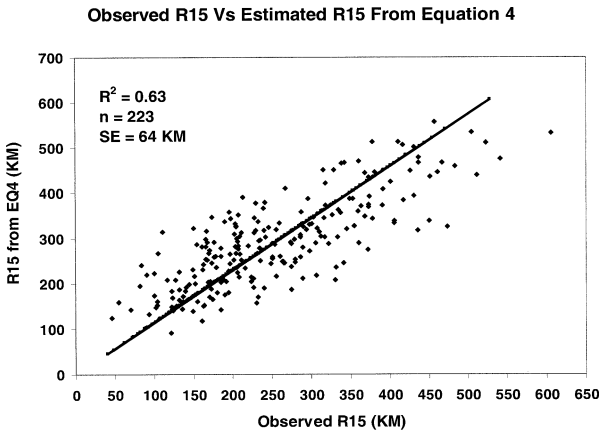

FIG. 14. Scatterplot and regression analysis for observed vs estimated [using Eq. (4)] values of R15.

Riehl (1954, 1963), and Shea and Gray (1973). The latter process entails calculating a scaling constant:

$$\text{Constant} = \text{VT} \cdot R^x, \tag{6}$$

where the exponent x was determined to be 0.5 (i.e., highest correlations in the observational data occurred for $x = 0.5$), VT is the range of tangential wind values of interest expressed in meters per second, and R is the radial distance from the TC center measured in kilometers. Once an estimate of R15 is obtained using Eq. (5), the estimated R15 is used to estimate R25 and R33:

$$\text{R25} = 0.36 \cdot \text{R15} \quad \text{and} \tag{7}$$

$$\text{R33} = 0.21 \cdot \text{R15}. \tag{8}$$

Table 5 gives a summary of results obtained in correlating observed R25 and R33 values versus estimated values obtained using Eqs. (7) and (8). Although the results are not as strong as those obtained for R15 using Eq. (5), they do indicate some skill in estimating R25 and R33. To test these equations further on an independent dataset, data for 15 TCs from the years 1986, 1996, and 1997 were collected and analyzed and where no gyre TCs were included. ''Observed'' values for R15 for each TC were derived using a combination of ship and island reports, aircraft reconnaissance (1986 only), and scatterometer data (1996 and 1997).

It would, moreover, be informative to compare this technique to techniques currently in use in the western Pacific. Presently, the JTWC uses a combination of climatological parameters to estimate a radius of 17.5 m s^{-1} winds (where R17 is a persistent artifact of 35-kt wind forecast technology) in lieu of in situ data such as ship and island reports or scatterometer measurements. One such method includes using infrared satellite imagery to infer the area of deep convection from cold (-65°C) cloud tops extending from the center of the TC as the approximate extent of R17. Another approach, the ''Huntley'' method, uses essentially the same parameters as this study (i.e., MCP and ROCI) to determine R17. During his tenure at JTWC, the first author often used Huntley methodology in the absence of scatterometer data and island observations. Unfortunately, attempts to find explicit documentation of the Huntley method and how it was derived were unsuccessful. Nevertheless, we used this technique for comparison with the procedures developed in the present study since relationships between R15 and satellite data observed in this study were poor.

TABLE 5. Category, number of observations, variance explained, and standard errors found between R25 and R33 as analyzed in the dataset and that predicted by Eqs. (7) and (8).

Category	No. of cases	Variance explained	Std errors (km)
R25 vs Eq. (4)	163	0.46	51.3
R33 vs Eq. (5)	120	0.34	34.6

As the Huntley method predicts values for R17 rather than the R15 considered herein, adjustments to the current technique involving Eqs. (5) and (7) were needed before comparisons were possible. Estimates of R17 were made by first using values of ER04 and MCP in Eq. (5) to calculate R15 values whereafter Eq. (7) was modified to convert R15 to R17, the latter resulting in

$$\text{R17} = 0.857 \cdot \text{R15}, \tag{9}$$

where both R17 and R15 are expressed in kilometers. Figures 15a,b show the results for R17 estimates obtained using the two methods versus actual observations. Figure 15a shows that R17 values estimated using Eq. (9) compared well with observations, yielding a value of variance explained of 66% and a standard error of about 60 km. The variance explained is essentially the same as for the developmental dataset. Figure 15b shows that the Huntley method also compared well to the observations, albeit with slightly more uncertainty, expressed as variance explained of 52% and a standard error of about 70 km. Actually, both techniques, derived independently of each other, utilize MCP and data on the size of the TC (i.e., ER04) in evaluating R17.

There were not enough observations of R25 and R33 to permit statistically meaningful testing of Eqs. (7) and (8) using the independent dataset. Nevertheless, the results show that a useful first approximation of the outer wind profile for western Pacific TCs can be diagnosed using either Eq. (5) or the Huntley method. These procedures may be quite useful to forecasters in the absence of scatterometer passes over TCs in the open (no islands) ocean. However, it must be understood that both techniques give only the average TC wind profile and do not consider structural asymmetries. Qualitative examination of the TC datasets revealed that there are significant outer wind asymmetries not associated with TC motion. The latter (asymmetries) might be an area for very fruitful research in coming years as more scatterometer data become available.

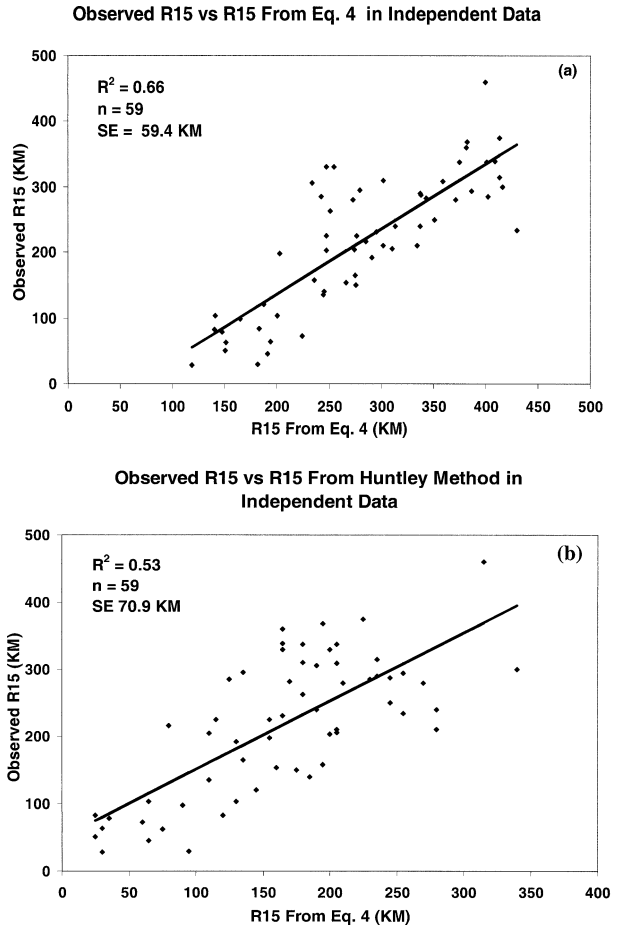

FIG. 15. (a) As in Fig. 14a but for the independent dataset. (b) As in (a) but using the Huntley method to diagnose R15.

6. Conclusions

Temporal variations of R15 and R25 were examined in conjunction with MCP wherein 43% of the TCs showed R15 changes (both positive and negative) of less than 50 km day^{-1}, 1.5 days prior to maximum intensity (i.e., during intensification). However, about 40% of the TCs did show significant R15 changes of greater than 50 km day^{-1} where about 20% of this variability occurred within 1.5 days prior to maximum intensity. Some of these R15 changes occurred during periods of rapidly falling MCP. These results are inconsistent with some earlier studies that suggested that the outer wind structure varies little during intensification. Changes in R25 were more difficult to assess reliably in the analysis due to sparse data.

Composites were made for classes of small, medium, large, and gyre cyclones. In general, the small TCs were indeed smaller than the medium and large TCs early on and throughout their respective composite life cycles. Large TCs had become significantly larger than medium and small TCs by the 25% point of the composite life cycles; these results collectively suggesting that specific synoptic environments affect TC size and special circumstances attend the formation of gyres. Composites of surface pressure fields around developing gyre and large TCs were significantly different when compared to the other TC categories; the most distinct differences were again seen for the gyre TCs.

Prospective relationships between R15 and several environmental parameters were examined for associations that might be useful for developing statistical prediction/analysis equations for estimating R15. The relationships between R15 and satellite-derived indices of convection were very weak, as found in previous studies. Estimates of the radius of the 1004-hPa isobar (termed ER04) were developed for the datasets as an alternative to the ROCI parameter. The ER04 parameter showed a significantly better relationship with R15 than did ROCI with good potential as a variable for multiple regression studies to estimate R15. Relationships between R15 and MCP in this study were found to be even poorer than observed in earlier studies. However, when the gyre TCs were removed from the dataset (15% of the observations), the relationship of R15 with MCP improved considerably.

A multiple regression relationship was developed using both ER04 and MCP to successfully estimate R15. Using these values for R15 and the Rankine vortex relationship, R25 and R33 could be estimated also. The skill for estimating R15 was good but only fair for R25 and R33. This technique was tested on an independent dataset and compared with the current (Huntley) technique used to estimate outer wind profile in the western Pacific. The results showed that, although both had different bias, both techniques have useful skill.

Acknowledgments. This study would not have been possible without the computer and drafting help of Barbara Brumit, Bill Thorson, and Judy Sorbee Dunn. Thanks to Drs. Ray Zehr, John Knaff, and Mark Lander for reviewing the paper. Finally, we would like to thank the U.S. Air Force Institute of Technology and the National Science Foundation (Grant ATM-0071369) for funding the authors' research.

REFERENCES

Brand, S., 1972: Very large and very small typhoons of the western North Pacific Ocean. *J. Meteor. Soc. Japan*, **50,** 332–341.

Carr, L. E., and R. L. Elsberry, 1997: Models of tropical cyclone wind distribution and beta effect propagation for application to tropical cyclone track forecasting. *Mon. Wea. Rev.*, **125,** 3190–3209.

Cocks, S. B., 1997: The outer radius tangential winds of tropical cyclones. M.S. thesis, Dept. of Atmospheric Science, Colorado State University, Fort Collins, CO, 102 pp.

Dvorak, V. F., 1975: Tropical cyclone intensity analysis and forecasting from satellite imagery. *Mon. Wea. Rev.*, **103,** 420–430.

——. 1984: Tropical cyclone intensity analysis using satellite data. NOAA Tech. Rep. NESDIS 11, Washington, DC, 47 pp.

Frank, W. M., and W. M. Gray, 1980: Radius and frequency of 15 m s^{-1} (30 kt) winds around tropical cyclones. *J. Appl. Meteor.*, **19,** 219–223.

Hawkins, J. D., and P. G. Black, 1983: SEASAT scatterometer detection of gale force winds near tropical cyclones. *J. Geophys. Res.*, **88,** 1674–1682.

Hughes, L. A., 1952: On the low level wind structure of tropical cyclones. *J. Meteor.*, **9,** 422–428.

IMSL, 1987: Fortran subroutines for statistical analysis. International Mathematical and Statistical Fortran Library, 1232 pp.

Lander, M. A., 1994: Description of a monsoon gyre and its effects on the tropical cyclones in the western North Pacific during August 1991. *Wea. Forecasting,* **9,** 640–654.

——, 1996: Specific tropical cyclone track types and unusual tropical cyclone motions associated with a reverse-oriented monsoon trough in the western North Pacific. *Wea. Forecasting,* **11,** 170–186.

Merrill, R. T., 1984: A comparison of large and small tropical cyclones. *Mon. Wea. Rev.,* **112,** 1408–1418.

Riehl, H., 1954: *Tropical Meteorology*. McGraw-Hill, 392 pp.

——, 1963: Some relations between wind and thermal structure of steady state hurricanes. *J. Atmos. Sci.,* **20,** 276–287.

Sadler, J. C., M. A. Lander, A. M. Hori, and L. K. Oda, 1987: *Pacific Ocean.* Vol. II, *Tropical Marine Climate Atlas,* Dept. of Meteorology, University of Hawaii, 20 pp.

Shea, D. J., and W. M. Gray, 1973: The hurricane's inner core region. I: Symmetric and asymmetric structure. *J. Atmos. Sci.,* **30,** 1544–1564.

Weatherford, C. L., 1985: Typhoon structural variability. Dept. of Atmospheric Science Paper 391, Colorado State University, Fort Collins, CO, 177 pp.

——, 1989: The structural evolution of typhoons. Dept. of Atmospheric Science Paper 446, Colorado State University, Fort Collins, CO, 198 pp.

——, and W. M. Gray, 1988a: Typhoon structure as revealed by aircraft reconnaissance. Part I: Data analysis and climatology. *Mon. Wea. Rev.*, **116,** 1032–1043.

——, and ——, 1988b: Typhoon structure as revealed by aircraft reconnaissance. Part II: Structural variability. *Mon. Wea. Rev.,* **116,** 1044–1056.

Zehr, R., 1987: The diurnal variation of deep convective clouds and cirrus with tropical cyclones. *Extended abstracts, 17th Tech. Conf. on Hurricanes and Tropical Meteorology,* Miami, FL, Amer. Meteor. Soc., 276–279.